Leading Basic Modes of Spontaneous Activity Drive Individual Functional Connectivity Organization in the Resting Human Brain

Xi Chen[a], Haoda Ren[a], Zhonghua Tang[a], Ke Zhou[b], Liqin Zhou[b], Zhentao Zuo[c], Xiaohua Cui[a], Xiaosong Chen[a], Zonghua Liu[d], Yong He[e,f,g,h], Xuhong Liao[a,f,*]

[a] School of Systems Science, Beijing Normal University, Beijing 100875, China;

[b] Beijing Key Laboratory of Applied Experimental Psychology, School of Psychology, Beijing Normal University, Beijing 100875, China;

[c] State Key Laboratory of Brain and Cognitive Science, Institute of Biophysics, Chinese Academy of Sciences, Beijing 100101, China;

[d] State Key Laboratory of Precision Spectroscopy, School of Physics and Electronic Science, East China Normal University, Shanghai 200241, China;

[e] State Key Laboratory of Cognitive Neuroscience and Learning, Beijing Normal University, Beijing 100875, China;

[f] Beijing Key Laboratory of Brain Imaging and Connectomics, Beijing Normal University, Beijing 100875, China;

[g] IDG/McGovern Institute for Brain Research, Beijing Normal University, Beijing 100875, China;

[h] Chinese Institute for Brain Research, Beijing 102206, China.

***Corresponding Author:** Xuhong Liao, Ph.D., School of Systems Science, Beijing Key Laboratory of Brain Imaging and Connectomics, Beijing Normal University, Beijing 100875, China; Tel/Tax: 8610-5880-7085; E-mail: liaoxuhong@bnu.edu.cn

Manuscript Information: 22 text pages, 4 figures

(Supplementary Information: 12 figures**)**

Abstract

Spontaneous activity of the human brain provides a window to explore intrinsic principles of functional organization. However, most studies have focused on interregional functional connectivity. The principles underlying rich repertoires of instantaneous activity remain largely unknown. We apply a novel eigen-microstate analysis to three resting-state functional MRI datasets to identify basic modes that represent fundamental activity patterns that coexist over time. We identify a few (i.e., five) leading basic modes that dominate activity fluctuations. Each of these modes exhibits a distinct functional system-dependent coactivation pattern and corresponds to specific cognitive profiles. In particular, the spatial pattern of the first leading basis mode shows the separation of activity between the default-mode and primary and attention regions. We further reconstruct individual functional connectivity as the weighted contribution of these leading basic modes based on theoretical modelling. Moreover, these leading basic modes capture sleep deprivation-induced changes in brain activity and interregional connectivity, primarily involving the default-mode and task-positive regions. Our findings reveal a dominant set of basic modes of spontaneous activity that reflect multiplexed interregional coordination and drive conventional functional connectivity, furthering the understanding of the functional significance of spontaneous brain activity.

Keywords: resting-state fMRI; low-dimensional representation; functional connectivity; cognitive function; sleep deprivation

Introduction

Spontaneous activity in the resting human brain exhibits well-organized spatiotemporal patterns, providing a window into understanding the intrinsic functional organization[1,2]. Using resting-state functional magnetic resonance imaging (R-fMRI), numerous studies have revealed the large-scale functional connectivity network by measuring low-frequency spontaneous fluctuations of blood-oxygenation-level-dependent (BOLD) signals[3-5]. The functional network exhibits non-trivial properties, such as functionally specific but interacting modules[6-8], which facilitate efficient functional segregation and integration across the brain[9-11]. Furthermore, the functional network architecture varies across individuals[12-15], shapes functional activation patterns during tasks[16-19], is related to individual cognitive performance[18,20,21], and is modulated by the mental states[22,23].

Despite the success of the functional network analyses, the associated insights are limited to the connectivity patterns summarized over time. Accumulating evidence suggests that the interregional functional interaction is highly dynamic with time-varying patterns[24-26]. An innovative approach is to examine single frames of brain activity to reveal the transient coordination at shorter time scales (e.g., seconds)[27]. The whole-brain activity patterns have been classified into a number of recurrent brain states with different coactivation patterns[28-30]. The temporal transition between these brain states follows a hierarchical structure[30] and shows alterations across tasks[31,32], consciousness states[33,34], and psychiatric disorders[35,36]. In addition to the group-level analysis, a very recent study has identified individualized brain coactivation states, the occurrence rates of which depend on task states, handedness, and gender, and show longitudinal changes in the post-stroke recovery[37]. Although these studies provide valuable insights into the time-varying functional organization, they typically assign the instantaneous activity pattern at each time point to a single brain state; the commonality shared across time points has been underestimated[38]. A more natural view holds that multiple basic modes may coexist across the time-resolved activity patterns, which are selectively combined at each time point to support future cognitive responses[26,39,40]. Identifying these basic modes can unravel building blocks of intrinsic activity and provide a new avenue to explore the multiplicity of the interregional relationships at rest. However, the spatial patterns of these basic activity modes and their potential functional significance remain largely unknown.

Recent R-fMRI studies have attempted to bridge the gap between instantaneous brain activity and functional connectivity (FC) patterns[28,41] For example, the point process analysis shows that FC profiles for regions of interest can be inferred from interregional coactivation patterns at specific time points[28,42]. Similarly, the edge-centric approach decomposes FC into the framewise contributions and reveals dominant contributions of high-amplitude coactivations at critical time points[41,43]. A recent study further reports that interregional FC relies on all time points, even those with low amplitudes[44]. Thus, we hypothesize that the basic modes of time-solved activity may make a substantial contribution to the FC pattern.

To address these issues, we leveraged a novel statistical physics approach, i.e., an eigen-microstate analysis[45], to identify the basic modes of spontaneous activity of the resting human brain. The eigen-microstate analysis is useful for extracting meaningful and fundamental spatial components (i.e., basic modes) that underlie the temporal evolution of complex systems[45]. Specifically, we applied this approach to R-fMRI data from healthy young adults from three datasets: the S900 release of the Human Connectome Project (HCP)[46], the sleep-deprivation dataset[47], and the Beijing Zang dataset[48]. First, we identified the leading basic modes that dominate the spontaneous fluctuations of BOLD signals and unraveled their cognitive significance. Second, we developed a theoretical model to elucidate how these basic modes contribute to the whole-brain FC pattern and verified this model by empirically reconstructing the FC pattern. Finally, we investigated whether these basic modes are affected by the modulation of mental states, e.g., by sleep deprivation.

Results

A small number of basic modes dominated spontaneous activity

We employed two runs (i.e., REST1 and REST2) of R-fMRI data from 700 participants selected from the HCP dataset and extracted regional time courses for 1000 cortical nodes based on a prior functional parcellation[49]. Then, we identified the basic modes at the population level for each run by applying the eigen-microstate analysis[45] to the concatenated time courses across participants (Fig. 1). For both runs, the weights of the basic modes decreased rapidly with increasing ranking and reached an elbow point at the 6th basic mode (Figs. 1A). The first five basic modes before the elbow point accounted for a large proportion of the variance in activity (29% for REST1 and 28% for REST2) ($p_{\text{perm}} < 0.001$, 10,000 permutation tests) and hereafter are referred to as the leading basic modes.

Each leading basic mode showed a heterogeneous spatial pattern, representing a typical fluctuation mode underlying rich repertoires of spontaneous activity (Fig. 1B); in the figure, opposite signs in the amplitude indicate opposite phases in the temporal fluctuation. The spatial patterns of these modes were highly similar between two runs (i.e., REST1 and REST2) (Fig. S1). Based on prior seven functional systems[50], we found that the spatial patterns of the leading basic modes were system-dependent (Figs. 1B and 1C). For basic mode 1, positive amplitudes were mainly located in regions of the default-mode and frontoparietal networks, whereas negative amplitudes were mainly located in regions of the somatomotor and visual networks, as well as those of the ventral and dorsal attention networks. This pattern is similar to the previously reported principal gradient of functional connectivity[51], suggesting a hierarchical separation of brain activity between transmodal regions and primary and attentional regions. For basic mode 2, positive amplitudes were mainly located in regions of the default-mode, somatomotor, and visual networks, while negative amplitudes were mainly located in the regions of the frontoparietal and ventral/dorsal attention networks. For basic mode 3, positive amplitudes were primarily located in

regions of the somatomotor, ventral attention, frontoparietal, and lateral default-mode networks, while negative amplitudes were primarily located in the visual and dorsal attention networks. For basic mode 4, positive amplitudes were mainly located in regions of the frontoparietal and dorsal attention networks, whereas negative amplitudes were mainly located in the ventral attention and medial visual networks. Basic mode 5 showed a finer spatial structure, in which heterogeneous amplitudes were observed within each functional system, and positive and negative amplitudes were mainly located in lateral and medial default-mode regions, respectively. These results suggest that a small set of basic modes govern the spontaneous fluctuations of brain activity, each of which shows a distinct coactivation pattern between functional systems.

We further identified the basic activity modes for each run at the individual level. We observed a small number of leading basic modes for most of the participants (number of leading basic modes, range: 3-10; mean ± std = 5.4 ± 1.39 for REST1 and mean ± std = 5.5 ± 1.39 for REST2) (Fig. S2).

Relationship between leading basic modes and cognitive functions

We examined whether spatial patterns of five leading basic modes were related to specific cognitive functions. First, we observed that these leading basic modes corresponded to different profiles of cognitive terms (Fig. 2A) based on the NeuroSynth meta-analytic database[52]. Basic mode 1 was positively associated with the default-mode related functions and negatively associated with sensorimotor and visual functions. Basic mode 2 was positively associated with the internally-oriented and social inference processes and negatively associated with working memory and task-oriented processes. Basic mode 3 was positively associated with sensorimotor, auditory, and language terms and negatively associated with vision-related functions. Basic mode 4 was positively associated with cognitively-demanding tasks (i.e., tasks, calculation, and objects) and negatively associated with pain-related terms. Basic mode 5 showed positive associations with the semantic-related functions and negative associations with the default-mode related functions.

We also examined the spatial similarity between the five leading basic modes and 12 cognitive components that represent the fundamental activation components during task performance[53] (Fig. 2B). Statistical significance of these spatial similarities was corrected for the spatial autocorrelation (all *p*s <0.05)[54]. Basic mode 1 was associated with internal mentation, emotion, interoception, and hand and face-related sensorimotor functions. Basic mode 2 was associated with several higher-order cognitive functions, including internal mentation, working memory, inhibition, interoception, and dorsal attention. Basic mode 3 was associated with both externally- and internally-oriented perceptions. Basic mode 4 was involved in working memory, dorsal attention, inhibition, reward, and interoception. Basic mode 5 was associated with visual, auditory and language functions. Overall, the first three leading basic modes are relevant to the internally-oriented, executive-control, and primary cognitive functions, whereas the latter two leading modes are related to more sophisticated and abstract functions.

Leading basic modes captured individual-specific functional connectivity patterns

Given that the leading basic modes served as the fundamental spatial components for whole-brain activity, we hypothesized that they would make dominant contribution to the whole-brain FC pattern and capture the individual-specific functional organization. To test this hypothesis, we developed a theoretical model based on the eigen-microstate analysis (Fig. 3A), which decomposed the whole-brain FC matrix into the weighted summation of the coactivation patterns in the basic modes. This model indicates that each basic mode corresponds to a specific FC pattern (Fig. S3). We reconstructed the whole-brain FC matrix based on this model by considering different numbers of basic modes and compared it with the original FC matrix obtained as Pearson's correlations between nodal time courses. At the population level, the spatial similarity between the reconstructed and original FC matrices slowly increased with the number of basic modes considered and then reached a plateau (Fig. 3A and Fig. S4). Specifically, we observed a high spatial similarity between two FC matrices when including the five leading basic modes (rs = 0.95 for both REST1 and REST2, ps < 0.001) (Fig. 3B and Fig. S4). Similar results were observed at the individual level. The spatial similarity between the reconstructed and original FC matrices was high for all participants when considering the five leading basic modes (Fig. 3C, mean ± std = 0.94 ± 0.02 for REST1 and 0.93 ± 0.02 for REST2).

We further evaluated whether the leading basic modes captured individual-specific functional organization. First, we found that the reconstructed FC matrix showed significantly higher values in the intra-subject similarity than inter-subject similarity, regardless of the number of basic modes used (Fig. 3D, all ps <0.05). Then, we performed the individual identification analysis[13] by comparing individual FC matrices between two runs. We observed an identification accuracy of 97% based on the original FC matrix. For reconstructed individual FC matrices, the identification accuracy increased rapidly with increasing number of basic modes and reached 92% when the five leading basic modes were included (Fig. 3E). These results suggest that these leading basic modes make the dominant contribution to the individualized functional organization.

Influence of sleep deprivation on the leading basic modes

To assess whether the leading basic modes are affected by the mental states, we applied the eigen-microstate analysis to the sleep-deprivation dataset[47]. In this dataset, 19 participants underwent R-fMRI scanning during rested wakefulness and after sleep deprivation. Similar to the HCP dataset, the weights of the basic modes at rested wakefulness decreased rapidly with increasing ranking and reached the elbow point at the 7th basic mode (Fig. 4A), indicating the presence of a small set (i.e., six) of leading basic modes (Fig. S5). These six leading basic modes showed a spatial correspondence with the first six basic modes of the HCP dataset, except for an inversion between basic mode 2 and basic mode 3 (Fig. 4A, all rs > 0.78).

Next, we evaluated the influences of sleep deprivation by comparing the leading basic modes between two mental states (i.e., at rested wakefulness and post-sleep deprivation). After the post-

sleep deprivation, we identified seven leading basic modes (Fig. 4B and Fig. S6). The spatial patterns of these seven basic modes showed a spatial correspondence between two states, except for an inversion between basic mode 4 and basic mode 5 (Fig. 4B). Notably, all these modes showed relatively low similarity values between two states, except for the first three modes and the 6th mode.

We further examined the difference in spatial patterns for the four basic modes (i.e., 1st, 2nd, 3rd, and 6th) that maintained spatial correspondences between two states. Significant changes in amplitude were observed in basic mode 1 (Fig. 4 C, $p_{\text{perm}} < 0.05$, false discovery rate (FDR) corrected). Significant increases were primarily located in regions of the frontoparietal, ventral and dorsal attention, and lateral visual networks, while significant decreases were mainly located in regions of the default-mode network. Interestingly, for most (86%) of these regions, the directions of the amplitude changes were opposite to the signs of the original amplitudes (Fig. S7), suggesting that the spatial inhomogeneity of brain activity was reduced after sleep deprivation. At the connectivity level, we also observed significant changes in the coactivation pattern of basic mode 1. The significant increase was mainly located between the default-mode network and the primary and attention networks, while the significant decrease was mainly located between the attention and the primary networks as well as within the default-mode network (Fig. 4D, $p_{perm} < 0.05$, FDR corrected), further supporting the reduction of cross-system inhomogeneity. Different from basic mode 1, no significant changes were observed for basic modes 2, 3 and 6 after sleep deprivation (all p_{perm}s > 0.05).

Validation results

We further assessed the reliability of the presence and spatial patterns of the leading basic modes (Figs. S8-S12). Four additional analysis strategies were considered, including (*i*) using stricter head motion exclusion criteria; (*ii*) performing nuisance regression without global signal regression; (*iii*) defining brain nodes based on two functional parcellations with different spatial resolutions; and (*iv*) using another independent dataset of 197 participants, i.e., the Beijing Zang dataset[48]. The presence of five leading basic modes was replicated with high spatial similarity in most of the cases (all rs > 0.85, Figs. S8, S10, and S11), except for the case of without global signal regression (Fig. S9). Notably, the total weight explained by the leading basic modes increased with the decreasing spatial resolution (Fig. S12), with weights of 37% and 44% for the 400-node and 200-node parcellations, respectively. For the strategy without global signal regression, the number of leading basic modes was reduced to four. The reduced number might be biased by the presence of an additional basic mode, which ranked ahead of the five typical basic modes. This additional basic mode showed all positive amplitudes across the brain and accounted for a large portion of activity variance (i.e., 23%) (Fig. S9). All these results suggest that the five leading basic modes were robust and reproducible.

Discussion

Using a novel eigen-microstate analysis from statistical physics theory, this study reveals the presence of a few leading basic modes that dominate the temporal fluctuations of spontaneous activity. The leading basic modes exhibited distinct and cognitive function-specific spatial patterns, suggesting the coexistence of multiplexed coactivation relationships between regions. Furthermore, these leading basic modes dominantly contributed to individual whole-brain FC patterns and were modulated by the sleep deprivation. Taken together, our findings highlight a small set of leading basic modes that dominate spontaneous activity and demonstrate their functional significance, opening a new avenue to explore the multiplexed interregional relationships in the healthy and diseased brain.

Leading basic modes reflects multiplexed coordination relationships between regions

Several approaches have been used to explore the typical coordination modes of spontaneous activity, such as classifying instantaneous activity patterns into brain states with different coactivation patterns[28,41,43] or revealing wave propagation patterns across regions[55,56]. In this study, we identified a small set of fundamental spatial components (i.e., leading basic modes) that dominate rich repertoires of spontaneous activity, regardless of datasets or mental states. These results suggest a reliable low-dimensional representation of seemingly complicated spontaneous activity. A low-dimensional representation of spontaneous activity has also been reported for rat cortical activity[57] and human brain activity across multiple task states[58]. We also found that each leading basic mode was associated with different cognitive functions. The first three leading basic modes were associated with fundamental functions that are necessary for daily life, such as sensorimotor, visual, internally-oriented, and executive-control functions. The next two leading basic modes were associated with more sophisticated and abstract cognitive functions, such as calculation, reward, and language-related items. These findings are consistent with previous hypotheses aimed at interpreting the biological significance of time-resolved activity patterns[24,40]. These hypotheses argue that spontaneous brain activity may transit between a number of general priors, which are low-dimensional representations of typical behavioral states in past experience[40] and are selected at different moments for an efficient and flexible cognitive response[24,40]. In this sense, the leading basic modes observed here might serve as the general priors, and their weights may reflect the frequencies of the corresponding behaviors in past experience.

Within the framework of the eigen-microstate analysis, distinct spatial patterns of these leading basic modes indicate the coexistence of distinct coactivation (i.e., coordination) patterns between regions. Interestingly, the first and second leading basic modes showed distinct relationships between the default-mode network, two cognitive control networks (i.e., frontoparietal and attention networks), and the primary networks. The first leading basic mode shows an anti-correlation primarily between the default-mode network and the primary and attention networks, which is highly similar to the previously reported spatial pattern of the principal gradient of the whole-brain FC pattern[51]. This finding suggests that the separation of

brain activity follows the hierarchical organization of information processing[59]. The second leading basic mode shows a separation of activity between the default-mode and cognitive control networks, which would explain the commonly observed alternative activities or anti-correlations between the default-mode and task-positive regions over time[55,60]. Compared to the previous assumption of one state per time point[30,61], the coexistence of multiple leading basic modes here suggests a parallel information processing between regions at each time point, providing novel insights into time-varying connectivity patterns[26].

The presence of the leading basic modes in intrinsic activity might be shaped by the anatomical substrates of the brain, given that the tight structure-function coupling of the brain[62,63]. For example, the first three leading basic modes here show a similar pattern to the myelination map of the brain[64], indicating a potential link between macroscale brain activity and the local microstructure. However, how these leading basic modes emerge from the anatomical properties, such as myelination, cortical thickness, and white-matter connectivity, requires further investigation.

Leading basic modes drive the functional connectivity pattern

Recent studies have reported that resting-state FC is driven by instantaneous brain activity at several critical time points[28,41], implicitly ignoring interregional coordination at other time points. Here, we used the leading basic modes, which were identified from full repertoires of spontaneous activity, to bridge the gap between instantaneous activity and the FC pattern. A theoretical model was developed to recover the FC pattern as a weighted superposition of the coactivation patterns of these leading basic modes. This model suggests that each basic mode corresponds to a specific FC pattern and that multiplexed relationships (i.e., parallel communication) exist simultaneously between regions. Our idea is consistent with a recent study showing that the individual FC pattern can be attributed to the contribution of multiple factors (e.g., group, individual, and task)[65], but it further clarifies the origins of FC patterns by providing detailed patterns of the candidate components. Interestingly, the five leading basic modes, which account for 29% of the total weight, can be used to reconstruct the original FC pattern with a high spatial similarity (r = 0.95). This seemingly contradictory finding suggests that these leading basic modes may capture the intrinsic coordination behavior of spontaneous activity, while the remaining basic modes may be vulnerable to unconstrained cognitive activity, head motion, or other perturbations, and thus make small contributions to interregional coordination. Furthermore, the spatial patterns of the first three leading basic modes are consistent with the patterns of the first three gradients of the cortical FC pattern[51], further solidifying the important role of these leading basic modes in shaping the FC pattern.

Moreover, we found that the reconstructed FC patterns based on the five leading basic modes captured individual uniqueness in functional organization, providing novel clues for understanding individual differences in functional organization. Notably, the FC pattern reconstructed by only the first leading basic mode was highly similar to the original pattern but showed a moderate

performance in individual identification. These results suggest that the first leading basic mode may serve as a backbone or a group factor of brain activity shared across individuals, as suggested by Ref[65]. Identification accuracy increased rapidly when subsequent basic modes were included, indicating that more individual-specific information is captured by subtly modulating the backbone of the FC pattern.

Leading basic modes are modulated by mental states

Sleep deprivation was used as a modulating factor to assess the influence of the mental state on the leading basic modes. A small number of leading basic modes were also identified after sleep deprivation, indicating the reliability of low-dimensional representations of spontaneous brain activity regardless of mental states. The spatial patterns of the first three and the sixth leading basic modes remained similar after sleep deprivation, whereas the other leading basic modes changed significantly. This finding is consistent with a recent study showing that the first three functional connectivity gradients remain largely unchanged after sleep deprivation[66]. Our results suggest that the activity representations relevant to fundamental cognitive functions might be reliable across mental states, while those related to more sophisticated and abstract functions may be more vulnerable. The different sensitivities of the leading basic modes to mental state may be valuable for future studies investigating functional organization across states.

In addition, a regional comparison revealed that the spatial heterogeneity of the first leading basic mode was reduced after sleep deprivation, manifested as a weakened separation of activity between the default-mode and task-positive areas (e.g., attention and somatomotor networks). This observation is confirmed by comparing the coactivation patterns corresponding to the first leading basic mode between two states. These results are consistent with previous findings suggesting that sleep deprivation is associated with the failure of the default-mode network to remain functionally distinct from its anti-correlated networks, i.e., task-positive networks[67-69]. This impairment in the decoupling between the default-mode network and task-positive networks may be further related to participants' cognitive vulnerability to sleep deprivation[68], but more evidence is needed to support this idea. Notably, the 4th and 5th leading basic modes showed remarkable reconfiguration after sleep deprivation. Given that these two modes are associated with sophisticated and abstract cognitive functions, the reconfiguration of these modes indicates the sensitivity of these functions to the sleep deprivation.

Further considerations

Several issues should be further considered. First, we identified an additional basic mode with all positive amplitudes when identifying the leading basic modes without global signal regression in the data preprocessing. This suggests that preserving the global signal may enhance coactivations between regions, providing a novel explanation for the usually observed rightward shift in the distribution of FC strength compared to the case with global signal regression[70]. Second, we explored the potential cognitive significance of leading basic modes through the association

analysis. In future studies, it is suggested to investigate the changes in the leading basic modes across task states to provide more direct clues. Third, additional leading basic modes were identified in the sleep-deprivation dataset, which may be influenced by several factors, such as the small sample size or mental states. A larger dataset is needed to further confirm the potential effects of sleep deprivation. Fourth, the biological origins of the leading basic modes remain unclear. Recent computational models of large-scale brain circuits have found that both interregional white matter connections and local circuit properties can shape resting-state functional connectivity and its itinerant dynamics[71,72]. In the future, the computational modelling approach can be used to explore the relationship between the leading basic modes and the underlying structural network and local morphological properties of the human brain. Finally, the eigen-microstate analysis used here is essentially a linear decomposition, which implicitly assumes that the rich repertoire of brain activity can be embedded in a low-dimensional linear subspace spanned by the leading basic modes. However, the biological plausibility of the low-dimensional nonlinear representation of spontaneous brain activity deserves further investigation.

Materials and methods

Participants and study design

We employed three datasets of R-fMRI data from healthy young adults. The first dataset consisted of multiband R-fMRI data from 970 participants from the publicly available S900 data release of the Human Connectome Project (HCP)[46]. These subjects underwent repeated R-fMRI runs in two sessions. The second dataset, named the sleep-deprivation dataset, included repeated R-fMRI data from 20 participants scanned separately during rested wakefulness and after sleep deprivation[47]. The third dataset, named the Beijing Zang dataset, included R-fMRI data from 198 participants selected from the 1000 Functional Connectomes Project[48]. Written informed consent was obtained from each participant. The first two datasets were used for the main analysis and the third dataset was used for the replication analysis.

Data acquisition

In the HCP dataset, all participants underwent multimodal MRI scanning with a customized 32-channel SIEMENS 3T Connectome Skyra scanner at Washington University, USA. Four multiband R-fMRI runs were acquired in two sessions for each participant. Briefly, each session consisted of two runs that were separately phases encoded in the left-to-right and right-to-left directions. The R-fMRI scans were obtained using a multiband gradient-echo-planar imaging sequence (repetition time [TR] = 720 ms and 1200 volumes per run, i.e., 14.4 min), with participants' eyes fixated on a bright projected crosshair. Here, we used only the left-to-right-encoded scans to reduce the potential influence of the phase-encoding directions[15,73]. In the original S900 data release, 837 participants completed the left-to-right-encoded R-fMRI scans in both sessions, denoted as REST1 and REST2 separately. Of these, 137 participants were excluded due to missing time points (N = 10), excessive head motion (N = 105) (see "Data Preprocessing"),

and arachnoid cysts (N = 22). Data from the remaining 700 participants (aged 21-35 years, M/F: 304/396) were used for the main analyses.

In the sleep-deprivation dataset, 20 participants underwent repeated R-fMRI scans separately during rested wakefulness and after sleep deprivation (for design details, see Zhou et al.[47]). All the participants were right-handed and had no history of neuropsychiatric disorders. The MRI data were acquired using a 64-channel 3T Siemens Prisma scanner at the Beijing MRI Center for Brain Research of the Chinese Academy of Sciences. R-fMRI data were acquired using a $T2^*$-weighted gradient-echo-planar imaging sequence (TR = 1000 ms and 480 volumes per run), with participants' eyes fixated on a crosshair. Structural images were acquired using a 3D T1-weighted, magnetization-prepared rapid acquisition gradient-echo sequence. One participant was excluded due to excessive head motion (see "Data Preprocessing"). Data from the remaining 19 participants (aged 18-26 years, M/F: 7/12) were used for the main analysis.

For the Beijing Zang dataset, 198 participants underwent MRI scanning using a 12-channel Siemens Trio Tim 3.0T scanner in the Imaging Center for Brain Research, Beijing Normal University. R-fMRI data were acquired with participants' eyes closed (TR = 2000 ms and 230 volumes). One participant was excluded due to differences in scanning orientation, leaving 197 participants (aged 18-26 years, M/F: 75/122) used for the cross-validation analysis.

Data preprocessing

For the HCP dataset, we employed the minimally preprocessed R-fMRI data[74], followed by ICA-Fix denoising[75]. Four additional steps were performed using the GRETNA package[76], including the removal of the first 10-second volumes (i.e., 15 volumes), linear detrending, nuisance regression, and temporal filtering (0.01-0.08 Hz). During the nuisance regression, white matter, cerebrospinal fluid, and global signals were included as regressors to further remove the influence of head motion and physiological noise[77].

The sleep-deprivation dataset and the Beijing Zang dataset were preprocessed with the same pipeline using the GRETNA package[76]. Specifically, the preprocessing included the removal of the first 10-second volumes, realignment, spatial normalization to the Montreal Neurological Institute (MNI) space with the T1-unified segmentation algorithm[78], linear detrending, nuisance regression, and temporal filtering (0.01-0.08 Hz). During the nuisance regression, we included Friston's 24 head-motion parameters[79], white matter, cerebrospinal fluid, and global signals as regressors to reduce the influence of head motion and physiological noise[77].

For these three datasets, we excluded participants with excessive head motion in any scan, including a translation/rotation greater than 3 mm or 3° and a mean framewise displacement (FD) over time[80] greater than 0.5 mm. After applying these criteria, 105 participants were excluded from the HCP dataset and 1 participant was excluded from the sleep-deprivation data.

Eigen-microstate analysis of spontaneous brain activity

We applied a novel eigen-microstate analysis[45] from the statistical physics theory to the HCP dataset to identify basic modes underlying rich repertoires of brain activity patterns. This approach has been applied to the temporal evolution of several complex systems (e.g., the Earth system and stock markets) and reveals well-defined spatial patterns that dominate their temporal fluctuations[45]. A similar approach has also been used to study the spatiotemporal patterns of brain oscillations in the visual cortex of rats[57]. In this study, the eigen-microstate analysis was applied separately to each R-fMRI run (i.e., REST1 and REST2). Nodal-level analyses were performed to reduce computational burden.

First, we defined 1000 cortical nodes (i.e., regions of interest) based on a prior functional parcellation[49] that would ensure functional homogeneity within each nodal region. We then extracted time courses of these nodes for each participant. The nodal time course for each node was further normalized by subtracting its mean value over time and then dividing by the corresponding standard deviation. Finally, the normalized nodal time courses were concatenated across participants, resulting in an $N\times M$ time course matrix A, where N denotes the number of nodes (i.e., 1000 here) and M denotes the number of time points in the concatenated time courses (i.e., 1185×700). Matrix A was considered as an ensemble matrix representing rich repertoires of brain activity patterns, and each column represents a microstate of brain activity from a statistical physics perspective.

The eigen-microstate analysis was performed by using singular value decomposition (SVD) as suggested in[45]. The ensemble matrix $A_{N\times M}$ was factorized as the product of three matrices:

$$A_{N\times M} = U_{N\times N}\Sigma_{N\times M}V^{T}_{M\times M}, \quad (1)$$

where $U_{N\times N}$ and $V_{M\times M}$ contain the columnar orthogonal bases in space (u_i) and time (v_i), respectively, and $\Sigma_{N\times M}$ is a diagonal matrix of singular values (σ_i). In this way, the time-varying brain activity pattern, A, can be viewed as the weighted combination of basic spatial modes (i.e., basic modes) u_i, accompanied by time-dependent coefficients v_i. The weight of each basic mode is characterized by σ_i^2, since the matrix A is normalized before SVD to ensure $\Sigma\sigma_i^2 = 1$. The normalization was performed by dividing the matrix A by the root sum square of all its elements (i.e., a dataset-dependent constant C).

To determine whether the brain is dominated by a small number of basic modes (i.e., low-dimensional representations), we identified leading basic modes, whose weights should be[81]: *i*) substantially greater than the weight of the subsequent basic mode, known as Cattell's scree test[82]; *ii*) greater than the average weight across all N possible basic modes, i.e., $1/N$; *iii*) statistically significant according to a permutation test. In each permutation instance, the labels of the nodal regions at each time point were randomly shuffled to disrupt the spatial organization. The statistical significance level of each leading basic mode was determined by comparing its original weight

(i.e., σ_i^2) to the null distribution of the corresponding weights obtained from the 10,000 permutation instances. In our analysis, the Cattell's scree test was performed by identifying the elbow point on the weight curve according to the Kneedle algorithm[83].

We further investigated the spatial patterns of the leading basic modes based on a prior functional system definition[50]. Seven systems were considered, including the default-mode network, frontoparietal network, limbic network, ventral attention network, dorsal attention network, somatomotor network, and visual network. For each leading basic mode, we estimated the mean fluctuation amplitude for each system by averaging the nodal values within this system.

We also performed the eigen-microstate analysis for each participant to investigate the presence of the leading basic modes at the individual level. In this condition, matrix A in Eq. (1) was replaced as the normalized time course within each participant for each R-fMRI run.

Cognitive function associations of the leading basic modes

We investigated the potential functional roles of the leading basic modes from two perspectives. First, we examined the association between these leading basic modes and cognitive functions based on the NeuroSynth meta-analytic database (www.neurosynth.org)[52]. For each leading basic mode, we calculated its spatial similarity with all available meta-analytic activation maps using Pearson's correlation across voxels. The associated cognitive terms are illustrated using word-cloud plots.

Second, we compared each of the leading basic modes with 12 cognitive components from[53]. Each cognitive component represents a basic activation probability map which is involved in various cognitive tasks[53]. For each cognitive component, we estimated the corresponding node-level version by averaging the activation probabilities of all voxels within each node. We then calculated the spatial similarity between each of the leading basic modes and the 12 cognitive components by using Pearson's correlation across nodes. To correct for the potential influence of spatial autocorrelation, the statistical significance of each spatial similarity was tested using the permutation test (n=10,000). The significance level was determined by comparing the original similarity to the null distribution of the corresponding similarity obtained from the 10,000 permutation instances. For each permutation instance, we generated a surrogate basic mode map that preserved the spatial autocorrelation of the original basic mode[54].

Relationship between leading basic modes and functional connectivity

Since the leading basic modes dominated the spontaneous fluctuations of brain activity, we further investigated how they contribute to the functional connectivity between regions.

The original FC between two nodal regions is defined as the Pearson's correlation between their time courses[4]. As each regional time course (A_{it}, $t = 1, \ldots M$) was normalized over time (i.e., mean = 0 and SD = 1), the FC between nodes i and j can be estimated as[13]:

$$FC_{ij} = \frac{1}{M-1}\sum_{t=1}^{M} A_{it}A_{jt}\,, \tag{2}$$

where M denotes the number of time points in the time course.

By substituting Eq. (1) into Eq. (2) and considering the time-independence between basic modes, we found FC_{ij} between nodes i and j can be rewritten as:

$$FC_{ij} = \frac{1}{M-1}\sum_{k=1}^{N} {\sigma_k}^2 u_{ki}u_{kj}\,, \tag{3}$$

where N is the number of all possible basic modes, and u_{ki} is the ith element of the kth basic mode. Thus, the functional connectivity between two nodes can be attributed to the joint contribution of their coactivation patterns in each basic mode. Notably, the FC_{ij} estimated from Eq. (3) should be further multiplied by a constant C^2 to correct for the normalization effect prior to the SVD analysis.

To validate the effectiveness of the above theoretical model (i.e., Eq. (3)), we reconstructed the FC matrix according to Eq. (3) by gradually increasing the number of basic modes of interest. We then compared the spatial similarity between the reconstructed and original FC matrices. The spatial similarity was quantified with Pearson's correlation across the lower triangular elements in the matrices. Specifically, we reconstructed the FC matrix at both the population and individual levels. At the population level, the leading basic modes were obtained from the concatenated normalized time course across all participants. At the individual level, the leading basic modes were identified from the time courses of each participant. We then calculated the similarity between the reconstructed and the original FC matrices for each individual.

We further explored whether the basic modes, especially these leading basic modes, could capture the individual functional organization. First, we estimated the reliability of the reconstructed FC matrix between two runs at the individual level. Given a participant of interest, we evaluated the intra-subject similarity of the reconstructed FC matrices between two runs. We also estimated the inter-subject similarity of this subject as the averaged spatial similarity of this participant in the first run (i.e., REST1) with all the other participants in the second run (i.e., REST2). Next, we examined the individual uniqueness in the reconstructed FC matrices by performing an FC-based individual identification analysis between two runs (i.e., REST1 and REST2)[13]. For each participant, we compared the reconstructed FC matrix of this participant in REST1 with those of all the participants in REST2. If the participant with the highest similarity in REST2 was the same participant given in REST1, the identification was correct; otherwise, it was incorrect. Identification accuracy was defined as the proportion of participants that were correctly identified. The higher the individual identification accuracy was, the more individual-specific information was captured in the analysis. For comparison, individual identification analysis was also performed based on the original FC matrix.

Influence of sleep deprivation on the leading basic modes

To assess whether the leading basic modes are affected by mental states, we applied the eigen-microstate analysis to a sleep deprivation dataset[47]. We identified the leading basic modes (see "Eigen-microstate analysis") separately from the R-fMRI data obtained in the two states represented in the dataset (i.e., rested wakefulness vs. post-sleep deprivation). First, we examined the spatial correspondence of the leading basic modes determined at rested wakefulness with those obtained from REST1 of the HCP dataset to investigate the reproducibility of the leading basic modes. Next, we compared the basic modes obtained at the different states (i.e., rested wakefulness vs. post-sleep deprivation) to examine the potential influence of the sleep deprivation.

For each leading basic mode that maintained spatial correspondence between two states, we tested differences in regional fluctuation amplitudes between the two states by using the permutation test (n = 10,000). In each permutation instance, the state labels of the R-fMRI data were shuffled for each participant. Multiple comparisons across nodal regions were corrected using the false discovery rate (FDR) approach (corrected $p < 0.05$)[84]. Given that the basic mode showed significant changes, we further investigated how interregional coactivation patterns differed between the two states. Briefly, we obtained the system-level coactivation pattern for the rested wakefulness and post-sleep deprivation separately. The within-system and between-system coactivation values were obtained by averaging the interregional coactivation values within the same system and between different systems, respectively. Significance levels of differences in the coactivation pattern were also estimated using the permutation test (n = 10,000) and corrected for multiple comparisons (FDR corrected $p < 0.05$).

Validation analysis

The reliability of the leading basic modes was validated by considering four analysis strategies that may affect the identification of the leading basic modes. In each case, the leading basic modes were re-estimated and compared with those obtained in the main analyses (i.e., REST1 in HCP). (*i*) Head motion. Head motion during R-fMRI scanning can affect the fluctuation amplitudes of BOLD signals[85]. Different from the main analysis, we used stricter head motion exclusion criteria for R-fMRI data in the HCP dataset (i.e., > 2 mm or 2° in any direction or mean FD > 0.2 mm) to further reduce the influence of head motion. (*ii*) Global signal regression. In the main analysis, the global signal was regressed to better reduce the influence of head motion and non-neural signals[77,85]. To assess the potential influence of the global signal, we re-preprocessed the R-fMRI data in the HCP dataset without global signal regression. (*iii*) Brain parcellation. To assess the influence of spatial resolution, we extracted regional time courses from the HCP dataset by using the same type of functional parcellations with different spatial resolutions (i.e., comprising 200 and 400 cortical regions)[49]. The leading basic modes obtained from different spatial resolutions were compared at the functional system level[50] and the voxel-wise level. In the latter case, the voxels within the same nodal regions were assigned the same amplitude values for each basic mode, regardless of the spatial resolution. In cases (*i*), (*ii*), and (*iii*), the validation analysis was performed

based on REST1 of the HCP dataset. (*iv*) Reproducibility across datasets. We identified the leading basic modes from another independent dataset, i.e., the Beijing Zang dataset[48], and compared them with those in the HCP dataset.

Data availability

The HCP dataset is publicly available at https://www.humanconnectome.org/study/hcp-young-adult/data-releases. The Beijing Zang dataset used for the replication analysis is publicly available at https://www.nitrc.org/projects/fcon_1000. Maps of leading basic modes and some other data supporting our results are available at https://github.com/chenxi000/Low-dimensional_representation_rsfMRI.

Code availability

Codes used for data analysis are available at https://github.com/chenxi000/Low-dimensional_representation_rsfMRI.

Acknowledgments

We thank Prof. Jingfang Fan for valuable discussion. This work was supported by the National Natural Science Foundation of China (Nos. 81971690 and 11835003), the Tang Scholar Award, and the Fundamental Research Funds for Central Universities (No. 2019NTST24).

Author contributions

X.C. and X.H.L. designed the research; Z.H.T., K.Z., L.Q.Z. and Z.T.Z collected parts of imaging dataset; X.C., H.D.R., X.H.C., X.S.C., Z.H.L., Y.H. and X.H.L. provided the methodological instruction; X.C. and X.H.L. performed the data analysis; X.C. and X.H.L. wrote the paper; X.C. and X.H.L. revised the paper.

Competing interests

The authors declare that there is no conflict of interest.

References

1. Fox MD, Raichle ME. Spontaneous fluctuations in brain activity observed with functional magnetic resonance imaging. *Nat. Rev. Neurosci.* **8**, 700-711 (2007).
2. Raichle ME. The restless brain. *Brain Connect.* **1**, 3-12 (2011).
3. Friston KJ. Functional and effective connectivity in neuroimaging: A synthesis. *Hum. Brain Mapp.* **2**, 56-78 (1994).
4. Biswal B, Yetkin FZ, Haughton VM, Hyde JS. Functional connectivity in the motor cortex of resting human brain using echo-planar MRI. *Magn. Reson. Med.* **34**, 537-541 (1995).
5. Kelly C, Biswal BB, Craddock RC, Castellanos FX, Milham MP. Characterizing variation in the functional connectome: promise and pitfalls. *Trends Cognit. Sci.* **16**, 181-188 (2012).
6. Achard S, Salvador R, Whitcher B, Suckling J, Bullmore E. A resilient, low-frequency, small-world human brain functional network with highly connected association cortical hubs. *J. Neurosci.* **26**, 63-72 (2006).
7. He Y*, et al.* Uncovering intrinsic modular organization of spontaneous brain activity in humans. *PLoS One* **4**, e5226 (2009).
8. Bertolero MA, Yeo BT, D'Esposito M. The modular and integrative functional architecture of the human brain. *Proc. Natl. Acad. Sci. U.S.A.* **112**, e6798-6807 (2015).
9. Bullmore ET, Bassett DS. Brain graphs: graphical models of the human brain connectome. *Annu. Rev. Clin. Psychol.* **7**, 113-140 (2011).
10. Bassett DS, Sporns O. Network neuroscience. *Nat. Neurosci.* **20**, 353-364 (2017).
11. Liao X, Vasilakos AV, He Y. Small-world human brain networks: Perspectives and challenges. *Neurosci. Biobehav. Rev.* **77**, 286-300 (2017).
12. Mueller S*, et al.* Individual variability in functional connectivity architecture of the human brain. *Neuron* **77**, 586-595 (2013).
13. Finn ES*, et al.* Functional connectome fingerprinting: identifying individuals using patterns of brain connectivity. *Nat. Neurosci.* **18**, 1664-1671 (2015).
14. Gordon EM*, et al.* Precision functional mapping of individual human brains. *Neuron* **95**, 791-807 (2017).
15. Liao X, Cao M, Xia M, He Y. Individual differences and time-varying features of modular brain architecture. *Neuroimage* **152**, 94-107 (2017).
16. Vatansever D, Menon DK, Manktelow AE, Sahakian BJ, Stamatakis EA. Default mode network connectivity during task execution. *Neuroimage* **122**, 96-104 (2015).
17. Schultz DH, Cole MW. Higher intelligence is associated with less task-related brain network reconfiguration. *J. Neurosci.* **36**, 8551-8561 (2016).
18. Cole MW, Ito T, Bassett DS, Schultz DH. Activity flow over resting-state networks shapes cognitive task activations. *Nat. Neurosci.* **19**, 1718-1726 (2016).
19. Tavor I, Jones OP, Mars RB, Smith SM, Behrens TE, Jbabdi S. Task-free MRI predicts individual differences in brain activity during task performance. *Science* **352**, 216-220 (2016).
20. Mill RD, Ito T, Cole MW. From connectome to cognition: The search for mechanism in human functional brain networks. *Neuroimage* **160**, 124-139 (2017).

21. Liu J*, et al.* Intrinsic brain hub connectivity underlies individual differences in spatial working memory. *Cereb. Cortex* **27**, 5496-5508 (2017).
22. Tagliazucchi E, Laufs H. Decoding wakefulness levels from typical fMRI resting-state data reveals reliable drifts between wakefulness and sleep. *Neuron* **82**, 695-708 (2014).
23. Chee MWL, Zhou J. Functional connectivity and the sleep-deprived brain. *Prog. Brain Res.* **246**, 159-176 (2019).
24. Deco G, Jirsa VK, McIntosh AR. Emerging concepts for the dynamical organization of resting-state activity in the brain. *Nat. Rev. Neurosci.* **12**, 43-56 (2011).
25. Hutchison RM*, et al.* Dynamic functional connectivity: promise, issues, and interpretations. *Neuroimage* **80**, 360-378 (2013).
26. Calhoun VD, Miller R, Pearlson G, Adali T. The chronnectome: time-varying connectivity networks as the next frontier in fMRI data discovery. *Neuron* **84**, 262-274 (2014).
27. Preti MG, Bolton TA, Van De Ville D. The dynamic functional connectome: State-of-the-art and perspectives. *Neuroimage* **160**, 41-54 (2017).
28. Liu X, Duyn JH. Time-varying functional network information extracted from brief instances of spontaneous brain activity. *Proc. Natl. Acad. Sci. U.S.A.* **110**, 4392-4397 (2013).
29. Liu X, Chang C, Duyn JH. Decomposition of spontaneous brain activity into distinct fMRI co-activation patterns. *Front. Syst. Neurosci.* **7**, 101 (2013).
30. Vidaurre D, Smith SM, Woolrich MW. Brain network dynamics are hierarchically organized in time. *Proc. Natl. Acad. Sci. U.S.A.* **114**, 12827-12832 (2017).
31. Chen JE, Chang C, Greicius MD, Glover GH. Introducing co-activation pattern metrics to quantify spontaneous brain network dynamics. *Neuroimage* **111**, 476-488 (2015).
32. Bray S, Arnold AE, Levy RM, Iaria G. Spatial and temporal functional connectivity changes between resting and attentive states. *Hum. Brain Mapp.* **36**, 549-565 (2015).
33. Di Perri C*, et al.* Multifaceted brain networks reconfiguration in disorders of consciousness uncovered by co-activation patterns. *Hum. Brain Mapp.* **39**, 89-103 (2018).
34. Huang Z, Zhang J, Wu J, Mashour GA, Hudetz AG. Temporal circuit of macroscale dynamic brain activity supports human consciousness. *Sci. Adv.* **6**, eaaz0087 (2020).
35. Yang H*, et al.* Reproducible coactivation patterns of functional brain networks reveal the aberrant dynamic state transition in schizophrenia. *Neuroimage* **237**, 118193 (2021).
36. Zhuang X, Walsh RR, Sreenivasan K, Yang Z, Mishra V, Cordes D. Incorporating spatial constraint in co-activation pattern analysis to explore the dynamics of resting-state networks: An application to Parkinson's disease. *Neuroimage* **172**, 64-84 (2018).
37. Peng X*, et al.* Robust dynamic brain coactivation states estimated in individuals. *Sci. Adv.* **9**, eabq8566 (2023).
38. Zhang X, Maltbie EA, Keilholz SD. Spatiotemporal trajectories in resting-state fMRI revealed by convolutional variational autoencoder. *Neuroimage* **244**, 118588 (2021).
39. Karahanoglu FI, Van De Ville D. Transient brain activity disentangles fMRI resting-state dynamics in terms of spatially and temporally overlapping networks. *Nat. Commun.* **6**, 7751 (2015).
40. Pezzulo G, Zorzi M, Corbetta M. The secret life of predictive brains: what's spontaneous activity for? *Trends Cognit. Sci.* **25**, 730-743 (2021).

41. Zamani Esfahlani F, *et al.* High-amplitude cofluctuations in cortical activity drive functional connectivity. *Proc. Natl. Acad. Sci. U.S.A.* **117**, 28393-28401 (2020).
42. Tagliazucchi E, Balenzuela P, Fraiman D, Chialvo DR. Criticality in large-scale brain fMRI dynamics unveiled by a novel point process analysis. *Front. Physiol.* **3**, 15 (2012).
43. Betzel RF, Cutts SA, Greenwell S, Faskowitz J, Sporns O. Individualized event structure drives individual differences in whole-brain functional connectivity. *Neuroimage* **252**, 118993 (2022).
44. Iraji A, *et al.* Moving beyond the 'CAP' of the Iceberg: Intrinsic connectivity networks in fMRI are continuously engaging and overlapping. *Neuroimage* **251**, 119013 (2022).
45. Sun Y, *et al.* Eigen microstates and their evolutions in complex systems. *Commun. Theor. Phys.* **73**, (2021).
46. Van Essen DC, *et al.* The WU-Minn Human Connectome Project: An overview. *Neuroimage* **80**, 62-79 (2013).
47. Zhou L, Tang Z, Zuo Z, Zhou K. Neural mechanism underlying the sleep deprivation-induced abnormal bistable perception. *Cereb. Cortex* **32**, 583-592 (2022).
48. Biswal BB, *et al.* Toward discovery science of human brain function. *Proc. Natl. Acad. Sci. U.S.A.* **107**, 4734-4739 (2010).
49. Schaefer A, *et al.* Local-global parcellation of the human cerebral cortex from intrinsic functional connectivity MRI. *Cereb. Cortex* **28**, 3095-3114 (2018).
50. Yeo BT, *et al.* The organization of the human cerebral cortex estimated by intrinsic functional connectivity. *J. Neurophysiol.* **106**, 1125-1165 (2011).
51. Margulies DS, *et al.* Situating the default-mode network along a principal gradient of macroscale cortical organization. *Proc. Natl. Acad. Sci. U.S.A.* **113**, 12574-12579 (2016).
52. Yarkoni T, Poldrack RA, Nichols TE, Van Essen DC, Wager TD. Large-scale automated synthesis of human functional neuroimaging data. *Nat. Methods* **8**, 665-670 (2011).
53. Yeo BT, *et al.* Functional specialization and flexibility in human association cortex. *Cereb. Cortex* **25**, 3654-3672 (2015).
54. Burt JB, Helmer M, Shinn M, Anticevic A, Murray JD. Generative modeling of brain maps with spatial autocorrelation. *Neuroimage* **220**, 117038 (2020).
55. Majeed W, *et al.* Spatiotemporal dynamics of low frequency BOLD fluctuations in rats and humans. *Neuroimage* **54**, 1140-1150 (2011).
56. Roberts JA, *et al.* Metastable brain waves. *Nat. Commun.* **10**, 1056 (2019).
57. Schiff SJ, Huang X, Wu JY. Dynamical evolution of spatiotemporal patterns in mammalian middle cortex. *Phys. Rev. Lett.* **98**, 178102 (2007).
58. Shine JM, *et al.* Human cognition involves the dynamic integration of neural activity and neuromodulatory systems. *Nat. Neurosci.* **22**, 289-296 (2019).
59. Mesulam MM. From sensation to cognition. *Brain* **121**, 1013-1052 (1998).
60. Fox MD, Snyder AZ, Vincent JL, Corbetta M, Van Essen DC, Raichle ME. The human brain is intrinsically organized into dynamic, anticorrelated functional networks. *Proc. Natl. Acad. Sci. U.S.A.* **102**, 9673-9678 (2005).
61. Allen EA, Damaraju E, Plis SM, Erhardt EB, Eichele T, Calhoun VD. Tracking whole-brain connectivity dynamics in the resting state. *Cereb. Cortex* **24**, 663-676 (2014).
62. Park HJ, Friston K. Structural and functional brain networks: from connections to cognition. *Science* **342**, 1238411 (2013).

63. Suarez LE, Markello RD, Betzel RF, Misic B. Linking structure and function in macroscale brain networks. *Trends Cognit. Sci.* **24**, 302-315 (2020).
64. Glasser MF*, et al.* A multi-modal parcellation of human cerebral cortex. *Nature* **536**, 171-178 (2016).
65. Gratton C*, et al.* Functional brain networks are dominated by stable group and individual factors, not cognitive or daily variation. *Neuron* **98**, 439-452 (2018).
66. Cross N*, et al.* Cortical gradients of functional connectivity are robust to state-dependent changes following sleep deprivation. *Neuroimage* **226**, 117547 (2021).
67. De Havas JA, Parimal S, Soon CS, Chee MW. Sleep deprivation reduces default mode network connectivity and anti-correlation during rest and task performance. *Neuroimage* **59**, 1745-1751 (2012).
68. Yeo BT, Tandi J, Chee MW. Functional connectivity during rested wakefulness predicts vulnerability to sleep deprivation. *Neuroimage* **111**, 147-158 (2015).
69. Krause AJ*, et al.* The sleep-deprived human brain. *Nat. Rev. Neurosci.* **18**, 404-418 (2017).
70. Murphy K, Fox MD. Towards a consensus regarding global signal regression for resting state functional connectivity MRI. *Neuroimage* **154**, 169-173 (2017).
71. Demirtas M*, et al.* Hierarchical heterogeneity across human cortex shapes large-scale neural dynamics. *Neuron* **101**, 1181-1194 (2019).
72. Wang P*, et al.* Inversion of a large-scale circuit model reveals a cortical hierarchy in the dynamic resting human brain. *Sci. Adv.* **5**, eaat7854 (2019).
73. Zalesky A, Fornito A, Cocchi L, Gollo LL, Breakspear M. Time-resolved resting-state brain networks. *Proc. Natl. Acad. Sci. U.S.A.* **111**, 10341-10346 (2014).
74. Glasser MF*, et al.* The minimal preprocessing pipelines for the Human Connectome Project. *Neuroimage* **80**, 105-124 (2013).
75. Griffanti L*, et al.* ICA-based artefact removal and accelerated fMRI acquisition for improved resting state network imaging. *Neuroimage* **95**, 232-247 (2014).
76. Wang J, Wang X, Xia M, Liao X, Evans A, He Y. GRETNA: a graph theoretical network analysis toolbox for imaging connectomics. *Front. Hum. Neurosci.* **9**, 386 (2015).
77. Yan CG*, et al.* A comprehensive assessment of regional variation in the impact of head micromovements on functional connectomics. *Neuroimage* **76**, 183-201 (2013).
78. Ashburner J, Friston KJ. Unified segmentation. *Neuroimage* **26**, 839-851 (2005).
79. Friston KJ, Williams S, Howard R, Frackowiak RS, Turner R. Movement-related effects in fMRI time-series. *Magn. Reson. Med.* **35**, 346-355 (1996).
80. Power JD, Barnes KA, Snyder AZ, Schlaggar BL, Petersen SE. Spurious but systematic correlations in functional connectivity MRI networks arise from subject motion. *Neuroimage* **59**, 2142-2154 (2012).
81. Misic B*, et al.* Network-level structure-function relationships in human neocortex. *Cereb. Cortex* **26**, 3285-3296 (2016).
82. Cattell RB. The scree test for the number of factors. *Multivar. Behav. Res.* **1**, 245-276 (1966).
83. Satopaa V, Albrecht J, Irwin D, Raghavan B. Finding a" kneedle" in a haystack: Detecting knee points in system behavior. In: *2011 31st international conference on distributed computing systems workshops*). IEEE (2011).

84. Benjamini Y, Hochberg Y. Controlling the false discovery rate: A practical and powerful approach to multiple testing. *J. R. Stat. Soc. B* **57**, 289-300 (1995).
85. Power JD, Schlaggar BL, Petersen SE. Recent progress and outstanding issues in motion correction in resting state fMRI. *Neuroimage* **105**, 536-551 (2015).

Figures

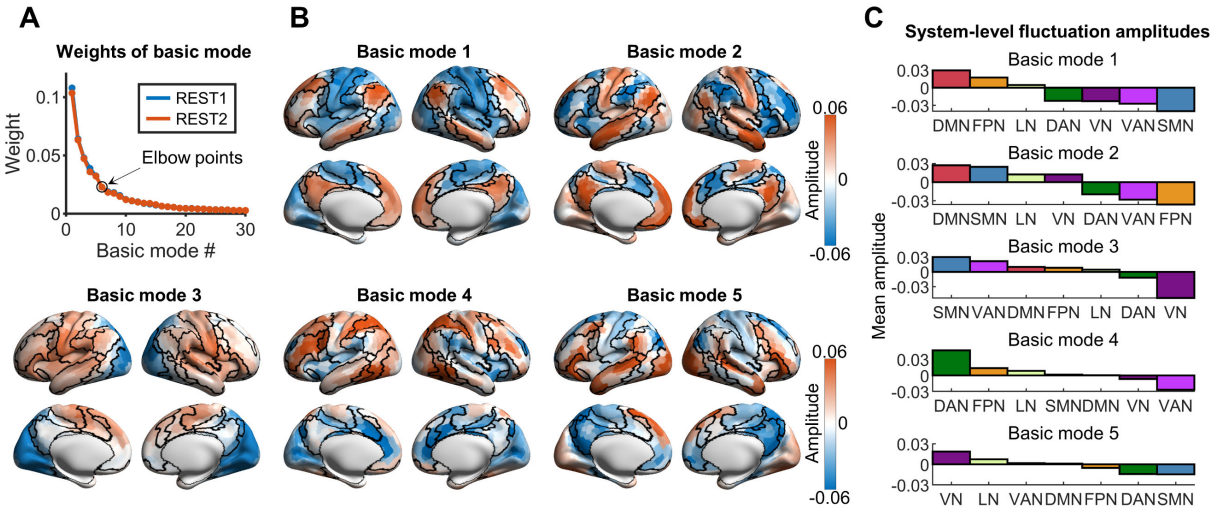

Figure 1. Leading basic modes of spontaneous brain activity. (A) Weights of basic modes for two runs (i.e., REST1 and REST2). The weights of the first thirty basic modes are displayed. Similar decreasing trends were observed for both runs. The first five basic modes were defined as the leading basic modes according to the criteria modified from[81]. (B) Spatial patterns of the first five basic modes (i.e., leading basic modes) for REST1. Black curves denote the boundaries of seven prior functional systems[50]. (C) System-level fluctuation amplitudes for the leading basic modes. Seven prior functional systems[50] were considered. DMN, default-mode network; FPN, frontoparietal network; LN, limbic network; VAN, ventral attention network; DAN, dorsal attention network; SMN, somatomotor network; VN, visual network.

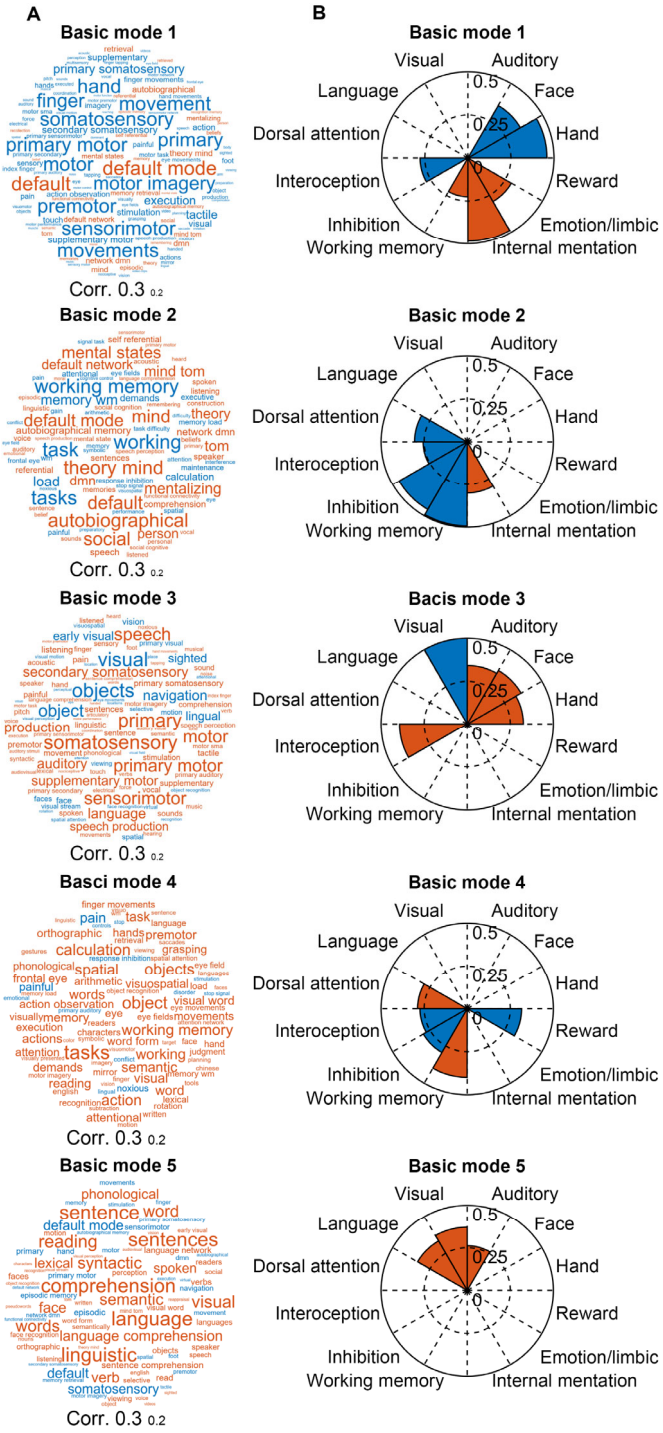

Figure 2. Association with cognitive functions. (A) Cognitive terms associated with each leading basic mode. These terms were obtained based on the NeuroSynth meta-analytic database[52]. Font sizes of cognitive terms denote correlation values between the corresponding cognitive term maps and the leading basic modes. (B) Associations with 12 cognitive components for each leading basic

mode. The 12 cognitive components were derived from Yeo et al.[53]. In (A) and (B), red and blue colors denote positive and negative correlations, respectively.

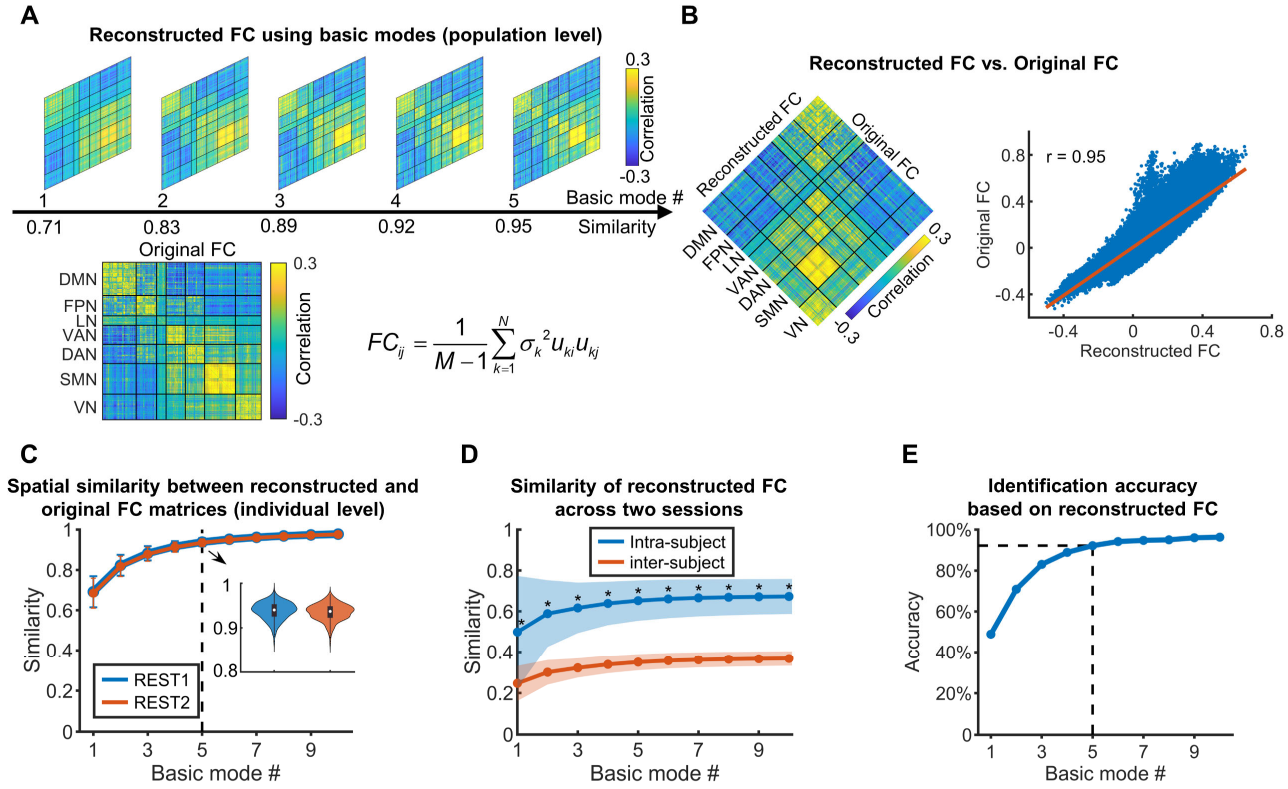

Figure 3. Reconstructing functional connectivity based on the basic modes. (A) Spatial similarity between the reconstructed and original FC matrices at the population level (REST1). The original FC matrix was estimated based on the concatenated time courses of all participants. The reconstructed FC matrix was generated separately by using different numbers of basic modes based on the theoretical model. (B) Reconstructing the FC matrix with the first five basic modes (REST1). Left, spatial patterns of the reconstructed and original FC matrices; right, spatial similarity between these two matrices. (C) Spatial similarity between the reconstructed and original FC matrices at the individual level for both runs. The reconstructed FC matrix was generated by using different numbers of basic modes. Mean spatial similarity across participants and the corresponding standard deviation are displayed. The distributions of individual spatial similarity obtained from the five leading basic modes are shown in the subplot in the form of the violin plots and the box plots. (D) Intra- and inter-subject similarity of the reconstructed FC matrices between two runs. *, denotes significant differences (paired *t*-tests, *p*s < 0.05). (E) Individual identification accuracy based on the reconstructed FC matrix. Individual FC matrices were reconstructed with different numbers of basic modes. FC, functional connectivity; DMN, default-mode network; FPN, frontoparietal network; LN, limbic network; VAN, ventral attention network; DAN, dorsal attention network; SMN, somatomotor network; VN, visual network.

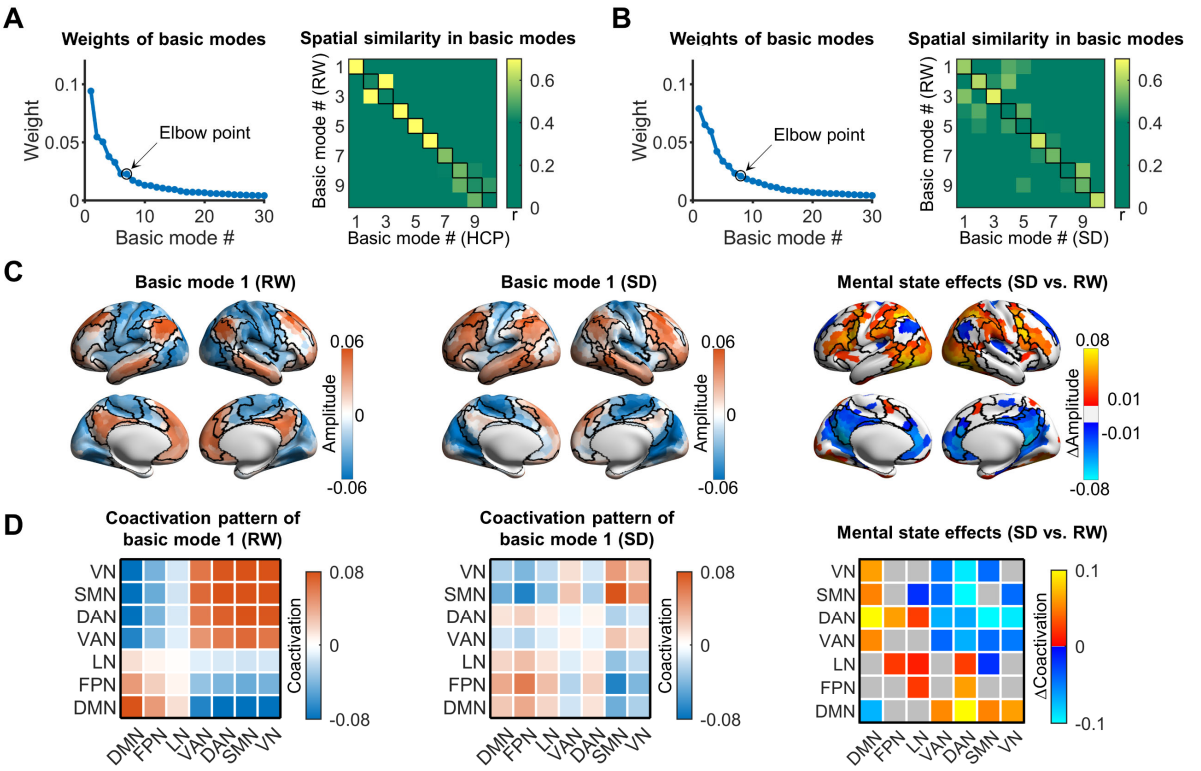

Figure 4. Influence of sleep deprivation on the basic modes in the sleep-deprivation dataset. (A) Weights of basic modes for R-fMRI data at rested wakefulness and spatial similarity of basic modes with REST1 in the HCP dataset. (B) Weights of basic modes for R-fMRI data after sleep deprivation and spatial similarity of basic modes with R-fMRI data at rested wakefulness. In (A) and (B), the spatial similarity was estimated for every pair of basic modes between two conditions to examine the spatial correspondence. (C) Spatial patterns of basic mode 1 at rested wakefulness and after sleep deprivation and their differences. Regions showing significant changes were detected with the permutation test ($p < 0.05$, FDR corrected). (D) System-level coactivation pattern of basic mode 1 at rested wakefulness and after sleep-deprivation and between-state differences. Significant changes were detected at the system level with the permutation test ($p < 0.05$, FDR corrected). RW, rested wakefulness; SD, after sleep-deprivation; HCP, Human Connectome Project.